American Mineralogist, Volume 89, pages 921–931, 2004

Hydroxyl in omphacites and omphacitic clinopyroxenes of upper mantle to lower crustal origin beneath the Siberian platform

MONIKA KOCH-MÜLLER,[1,*] STANISLAV S. MATSYUK,[2] AND RICHARD WIRTH[1]

[1]GeoForschungsZentrum Potsdam Telegrafenberg 14473 Potsdam
[2]Institute of Geochemistry, Mineralogy and Ore Formation, Ukrainian Academy of Science, Pr. Palladina 34, Kiev-252 142

ABSTRACT

A series of clinopyroxenes from the lower crust and upper mantle beneath the Siberian platform was investigated by Fourier-transform infrared (FTIR) spectroscopy and transmission electron microscopy (TEM). The IR spectra of all our samples exhibit three groups of absorption bands at (1) 3445–3465, (2) 3500–3540, and (3) 3600–3624 cm^{-1}. Using synchrotron IR radiation, which utilizes a spot size of only 5×5 μm, we realized that the intensities of the absorption bands, mostly those of group 3, showed extreme variation within one crystal. TEM as well as polarized and high-pressure IR spectroscopy indicated that the OH groups that cause the bands of group 3 were not intrinsic but due to nm-sized inclusions of sheet silicates.

The intensities and peak positions of the bands of group 2 correlate with the amount of tetrahedral Al^{3+} indicating that the charge-deficient substitution of Al for Si is responsible for the bands of group 2. The intensities and peak positions of the bands of group 1 correlate with the concentration of vacancies at M2 indicating that the cation vacancies at M2 control the incorporation of hydroxyl responsible for the bands of group 1. The bands of groups 1 and 2 are caused by the same type of OH dipole, however, occurring in different structural environments.

The concentration of the structurally bound water of the omphacitic clinopyroxene is in the range from 31 to 514 ppm H_2O (by weight). Surprisingly, the lowest concentration was found in clinopyroxene, that comes from the highest pressure region, i.e., the diamond-bearing eclogite xenoliths of the Mir kimberlite pipe. The highest values were obtained in omphacites of the lower-pressure grospydites of the Zagadochnaya kimberlite pipe and in omphacitic clinopyroxene of the lower pressure granulites of the Udachnaya kimberlite pipe, respectively. The low water content of clinopyroxene from the high-pressure region seems to be controlled by low water activity during crystallization. However, hydrogen loss during the uplift cannot be ruled out.

INTRODUCTION

Clinopyroxene (cpx) is a major constituent of the Earth's crust and mantle. From experimental studies (e.g., Skogby and Rossman 1989; Skogby 1994; Bromiley and Keppler 2003) as well as from studies of natural systems (e.g., Skogby et al. 1990; Smyth et al. 1991; Beran et al. 1993; Bell et al. 1995; Peslier et al. 2002; Katayama and Nakashima 2003) it is well known that cpx can store hydrogen in its structure. Hydrogen concentration varies widely from 100 to 1300 ppm H_2O (by weight in this paper) as a function of geological setting with the largest concentration occurring in mantle-derived omphacites (e.g., Skogby et al. 1990; Rossman 1996). In a recent study of an omphacite from a diamond-grade eclogite from the Kokchetav massif, Kazakhstan, Katayama and Nakashima (2003) reported water contents as high as 3000 ppm H_2O.

Three groups of OH-stretching bands can be distinguished in omphacites from eclogites: (1) 3445–3465, (2) 3500–3540, and (3) 3600–3624 cm^{-1}. The bands of group 1 and 2 are usually the strongest in the spectra whereas those of group 3 are very weak (Skogby et al. 1990; Beran et al. 1993; Smyth et al. 1991). However, the infrared spectra of the OH-richest omphacite known so far (Katayama and Nakashima 2003) are different from those previously published. They show bands of group 3 that are extremely intense, even more intense than those of groups 1 and 2.

In the clinopyroxene structure, the O2 site is the most favorable location for OH substitution (Beran 1976; Cameron and Papike 1980; Smyth 1989). The substitution of O^{2-} by OH^- may be balanced by either cation vacancies (e.g., Smyth et al. 1991) or a charge-deficient substitution such as trivalent ions for Si (e.g., Skogby et al. 1990; Skogby 1994). Smyth et al. (1991) showed that intensities of the bands of group 1 in upper-mantle cpx from the Roberts Victor kimberlite pipe correlate with M2 site vacancies (corresponding to a Ca-Eskola component, $Ca_{0.5}\square_{0.5}AlSi_2O_6$). An increase in the number of M2 site vacancies with increasing hydroxyl concentrations and increasing pressure of recrystallization of the host rocks also was observed by Katayama and Nakashima (2003) for the Kokchetav UHP clinopyroxenes. However, trivalent cations have been shown to be correlated only weakly with the intensity of the groups 1 and 2 bands (Skogby et al. 1990).

Our aim was to study cpx from different xenoliths from the lower crust and upper mantle beneath the Siberian platform with respect to their hydrogen concentration and the type of OH-defects.

* E-mail: mkoch@gfz-potsdam.de

0003-004X/04/0007–921$05.00

Sample selection and petrological settings

We selected omphacites from eight eclogite samples and omphacitic cpx (<20 mol% jadeite component) from two granulite samples from four Yakutian kimberlite pipes in order to investigate the hydroxyl content of cpx from different *P-T* conditions beneath the Siberian platform (Table 1). The highest *P-T* grade was observed for the samples of diamond-grade eclogite from the Mir kimberlite pipe (TM-8, A-45/2 first described by Sobolev 1974) for which a pressure estimate of 4.4–5.5 GPa at a temperature between 1000–1200 °C has been made (Ukhanov et al. 1988). The lowest grade was observed for the granulite samples from the Udachnaya pipe for which a *P* estimate of 1.2–2.0 GPa at 900–1100 °C was made (Spetsius and Serenko 1990). The xenoliths are well characterized (Table 1). We hand picked crack-free and optically clear cpx from the host xenoliths. The selected crystals are several hundred micrometers in diameter and green to gray in color. Most parts of the single crystals are optically clear but careful optical microscopy showed the presence of solid inclusions ranging in size from mm to µm in some parts of the individual crystals. The inclusion-rich parts are located at the rims of the crystals and/or along cleavage planes, and/or they form veins within the optically clear parts.

Analytical techniques

Electron microprobe analyses

The Electron microprobe (EMP) analyses of the clinopyroxenes were performed with Cameca SX50 and SX100 instruments at the GeoForschungsZentrum Potsdam using the wavelength-dispersive mode. The operating conditions were 15 kV and 20 nA. Counting times was set at 20 s on peak and 10 s on background. Well-characterized natural minerals were used as standards: diopside (Si, Ca), K-feldspar (Al, K), olivine (Mg), albite (Na), hematite (Fe), rhodonite (Mn), rutile (Ti), and chromite (Cr). Raw spectrometer data were corrected with the PAP program (Pouchou and Pichoir 1985).

TEM and AEM

Individual single crystals were checked for the presence of nanometer- or submicrometer- sized inclusions by TEM in combination with analytical electron microscopy (AEM) (samples:U-74, O-175/87, Tw-297/77 Ol-288/74). Site specific TEM foils were prepared by the Focused Ion Beam technique (FIB) (Fig. 1) using a FEI FIB200 instrument at the GFZ. Details of the FIB technique are given elsewhere (Overwijk and van den Heuvel 1993; Heany et al. 2001). The final thickness of the TEM foils was about 120 nm. The foils were removed from the sample using a manipulator with a glass fiber under an optical microscope, and placed onto a perforated TEM carbon grid. No further carbon coating was required. One sample was prepared by conventional argon ion milling (O-175/87).

TEM was performed with a Philips CM200 transition electron microscope operating at 200 kV and equipped with a LaB_6 electron source. The TEM is equipped with a Gatan imaging FilterGIF and an energy dispersive EDAX X-ray spectrometer with ultrathin window. Energy filtered images were acquired by applying a 10 eV window to the zero loss peak.

Infrared spectroscopy

At least two wafers were prepared from each sample, one in (010) orientation and the other in (100) orientation. The mineral orientation was determined by optical microscopy. Each side of the wafers was given a final polish using a diamond paste (grain size = 0.8 µm). The thickness of the grains ranged from 100 to 400 µm, which was measured with a digital micrometer. To determine the hydroxyl concentrations accurately, we measured polarized infrared spectra parallel to the three indicatrix axes. The (010) wafer was used to obtain spectra with the electric field vector E parallel to n_γ and n_α and the (100) wafer for n_β. The measurements were performed at the GeoForschungsZentrum Potsdam and the Technische Universität Berlin using a Bruker ISF 66v FTIR spectrometer coupled with an IRScope microscope and a KRS-5 polarizer. The spectra were acquired in optically clear parts with an aperture diameter ranging from 50 to 150 µm and a spectral resolution of 2 cm^{-1}. The weak but sharp absorption bands between 3600 and 3700 cm^{-1} in some of the spectra are due to atmospheric H_2O vapor.

To quantify the water content of the samples, the areas beneath the O-H stretching bands were integrated for all three principal directions of the optical indicatrix (A_α, A_β, A_γ) using the software Peakfit (Jandel Scientific). We only considered the absorption peaks of the groups 1 and 2 bands in the quantification, not those of group 3 because we know that the corresponding OH groups are not intrinsic but belong to nanometer-sized inclusion of sheet silicates, mainly clinochlore (see below). For samples with a high concentration of these inclusions (e.g., sample O-175), this method overestimates the water content by about 7% as we neglected the contribution of the non-intrinsic bands to the intensity of the bands of groups 1 and 2 in the water calculations. We applied a Gaussian plus Lorentzian distribution function to all component bands. The H concentration, given as wt% H_2O, was calculated using the equation C_{H2O} (wt%) = $(1.8 \cdot A_{i,tot})/(\rho \cdot \varepsilon_i \cdot t)$, with $A_{i,tot} = (A_\alpha + A_\beta + A_\gamma)$, ε_i = integrated molar absorption coefficient [cm^{-2} per mol H_2O /L], t = thickness [cm] and ρ = density (g/cm^3). However, quantitative determination of hydrogen contents of omphacites from infrared spectra is problematic because no mineral-

Table 1. Samples, localities, *P*, and *T* estimates and water contents

Sample no.	Locality in Yakutia	Rock	Paragenesis*	*P*, GPa	*T*, °C	References	wt ppm H_2O‡
TM-8	Mir	D-bearing eclogite	Gt_{25-30} + Cpx_{70-75} + D	4.4	1205	Ukhanov et al. (1988)	31 (61)
A-45/2	Mir	D-bearing eclogite	Gt_{25-30} + Cpx_{70-75}+Ru + G + D	5.5	988	Ukhanov et al. (1988)	60 (116)
Tw-297/77†	Udachnaya	Eclogite	Gt_{40-42} + Cpx_{58-60}	3.9–4.3	1050–1300		61 (119)
Tw-140/79†	Udachnaya	Eclogite	Gt_{35-40} + Cpx_{60-65}	3.9–4.3	1050–1300		146 (284)
2290	Udachnaya	Coesit-eclogite	Gt_{42}+ Cpx_{48}+ Co_5+ Ky_4+ $Ru_{0,5}$ + $Slf_{tr.}$	3.0	1010–1020	Spetsius (1990)	152 (268)
Ol-288/74	Obnazhonnaya	Cd-eclogite	Gt_{25-30} + Cpx_{50-55} + Cd_{10-15}	3.0	1350–1400	Qu et al. (1997)	448 (760)
O-175/87	Obnazhonnaya	Cd-eclogite	Gt_{25-30} + Cpx_{30-35} + Cd_{30-35}				466 (792)
Zg-25/78	Zagadochnaya	Grospydite	Gt_{50} + Cpx_{15} + Ky_{35}	<3.0	1200	Sobolev (1974)	504 (886)
U-74	Udachnaya	Ky-granulite	Gt + Cpx + Ky + Pl	1.3–2.0	900–1100	Spetsius and Serenko (1990)	437 (748)
U-935	Udachnaya	Cd-granulite	Gt_3 + Cpx_{27} + Cd_4 + $Ky_{tr.}$ + Pl_{62} + Sc_3	1.3–2.0	900–1100	Spetsius and Serenko (1990)	514 (872)

*For abbreviations of mineral phases: Amph = amphibole, Cd = corund, Co = coesite, Cpx = clinopyroxene, D = diamond, G = graphite, Gl = glaukophane, Gt = garnet, Opx = orthopyroxene, Pl = plagioclase, Q = quarz, Ky = kyanite, Ms = muscovite, Ru = rutile, Slf = sulphide, Sc = scapolite; tr. = traces.
† *P, T* calculated after Raheim and Green (1974).
‡ Water content calculated using the general IR absorption calibration of Libowitzky and Rossman (1997). The values in parenthesis correspond to water contents calculated using the absorption coefficients for Cpx as determined by Bell et al. (1995).

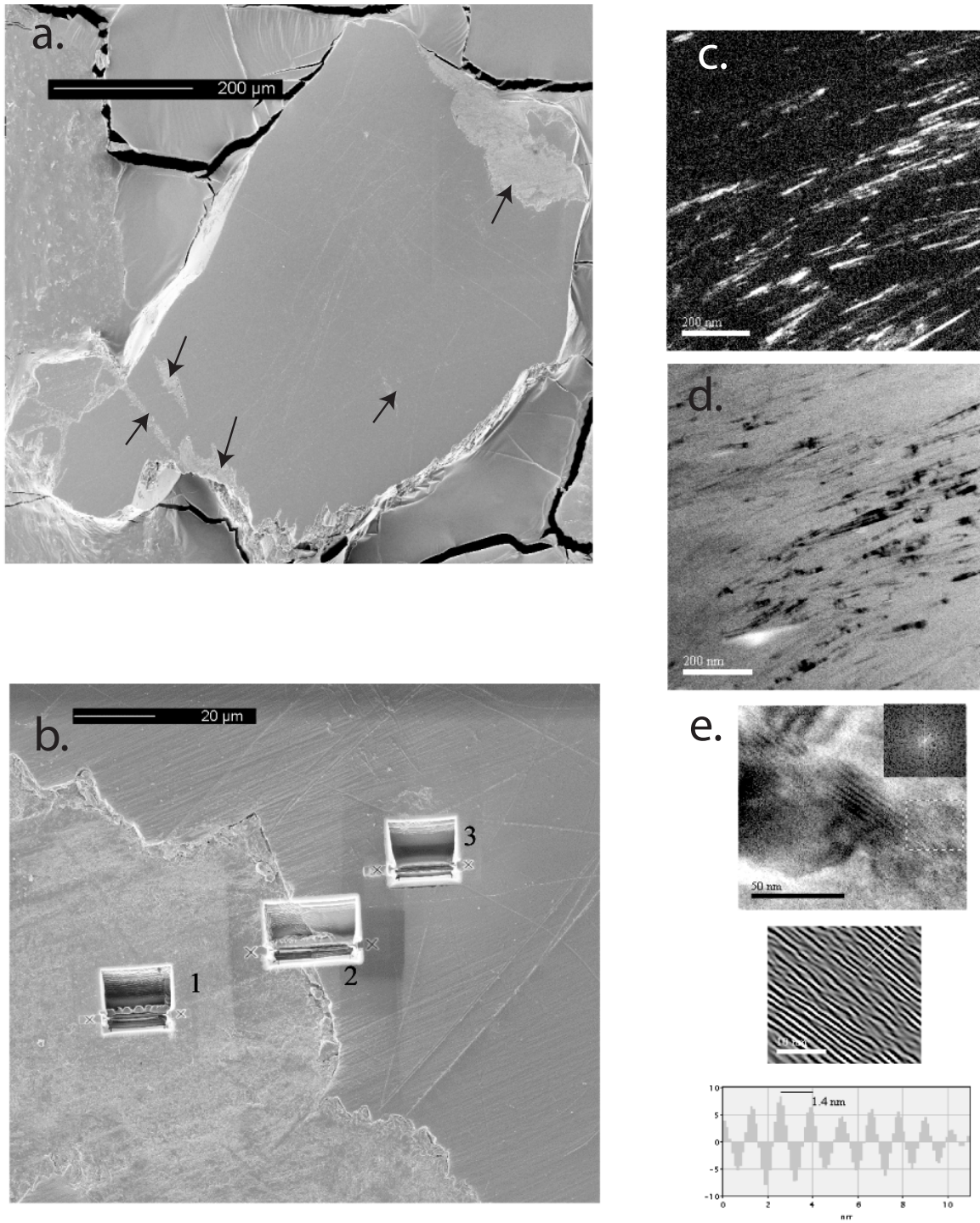

FIGURE 1. (a) SE image of a particular omphacite grain. The arrows highlight the inclusion-rich parts. **2** SE image of the grain in Fig.1a at higher magnification. The grooves where the TEM foils have been cut by the FIB technique are visible and labeled 1–3. The TEM foils are already removed. Groove 1 is located in an area with many tiny inclusions, groove 2 covers an inclusion-rich part (left) plus an inclusion-free part (right), and groove 3 is located in an optically inclusion-free part of the omphacite. **(c)** Energy filtered, dark-field image of sheet silicate inclusions in omphacite using an (00l) reflection of the sheet silicates. **(d)** Corresponding energy filtered, bright-field image. **(e)** Energy filtered, HREM image with lattice fringes and the corresponding diffraction pattern inserted (Fast Fourier Transform FFT). The Fourier-filtered image (inverse of the FFT) represents the area indicated in the original image. The trace of the intensity profile across the Fourier-filtered image is indicated and the corresponding plot gives a lattice fringe spacing of 14 Å.

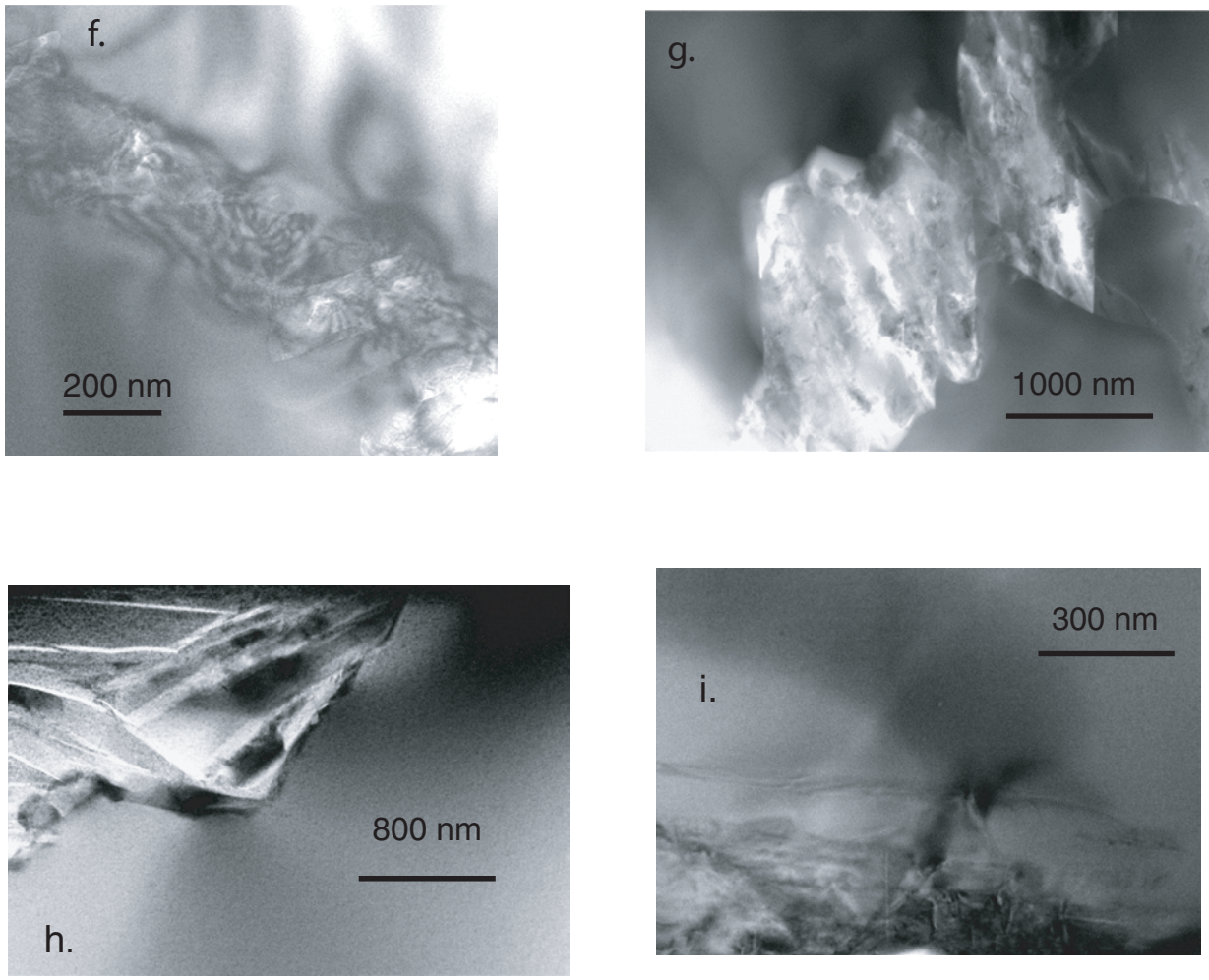

FIGURE 1 CONTINUED. (f) TEM bright-field image showing a narrow vein (200–400 nm) of sheet silicates in omphacite. **(g)** Another vein of sheet silicates in omphacite. Note the sharp and crystallographically oriented reaction fronts. **(h, i)** TEM bright-field images of sample U-74 showing biotite inclusions.

specific calibration has been published so far (Ingrin and Skogby 2000). There are reliable absorption coefficients for diopside and augite (Skogby et al. 1990; Bell et al. 1995) but not for omphacite. By applying the coefficient for diopside or augite to quantify the water content in omphacite, one could overestimate the water content because omphacite spectra are significantly different from those of diopside and augite with the main absorption being at lower wavenumbers. Here we followed the suggestions of Ingrin and Skogby (2000), i.e., we applied the general calibration method by Libowitzky and Rossman (1997) to quantify the water content. If we take the absorption coefficient for cpx as determined by Bell et al. (1995) instead of the calibration by Libowitzky and Rossman (1997), the water contents would be twice as much (Table 1). Thus, in the lack of an appropriate ε-value for omphacite, it is meaningless to discuss absolute water contents but we can use the calculated ones to compare the water content of different omphacites in relation to their geological settings.

To determine the orientation of the corresponding OH dipoles, the angular relations between the direction of n_γ in the (010)-plates and the electric field vector E were changed from 0–180° for some of the samples and absorbances were measured in steps of 10°. This procedure is only necessary for monoclinic and triclinic crystals. In crystals of higher symmetry, the maximum and minimum absorbance of symmetry related OH dipoles are always parallel to the indicatrix axes and the orientations of the OH dipoles can be calculated from these data.

To check whether the bands of group 3 obtained in optically clear parts of the omphacite crystals are really related to nanometer-sized inclusions of clinochlore, in-situ high-pressure FTIR spectra on omphacite and clinochlore were recorded and the response of the OH bands to changes in pressure was compared. The spectra were collected on a Bruker ISF 66v FTIR spectrometer at the GeoForschungsZentrum Potsdam. We used a Megabar-type diamond-anvil cell (Mao and Hemley 1998) with type II diamonds and a stainless steel gasket. An omphacite crystal, 100 × 80 × 50 µm in size, and ruby grains were embedded in the gasket hole (diameter of 300 µm) with CsI as a pressure medium. The aperture was set to 70 µm in diameter. The pressure was determined from the energy shift of the R_1 ruby fluorescence line relative to its energy at ambient conditions (Mao et al. 1986). In-situ high pressure FTIR spectra of a synthetic Mg-rich chlorite powder, 99-1 (Koch-Müller and Wirth 2001) were acquired using the same set up as described above.

To check the homogeneity of the samples with respect to the distribution of the OH groups, several spectra were taken on different parts of the crystals with a spatial resolution of 5 × 5 µm. The spectra were recorded at the synchrotron IR-beamline at Bessy II in Berlin, Germany, using a Nicolet 870 FTIR spectrometer equipped with a Continuum microscope. Because of the brilliance of the synchrotron light, unpolarized as well as polarized spectra could be collected with such a small aperture.

RESULTS AND DISCUSSION

Composition of the clinopyroxenes and their inclusions

Table 2 lists the chemical compositions of the clinopyroxenes investigated here. Individual grains of each sample are chemi-

cally very homogenous, however, the compositions of all cpx are variable. The change in composition from sample to sample clearly reflects the different geological settings. Low jadeite components ($NaAlSi_2O_6$) were observed in the low-*P* cpx and high jadeite component in diamond-grade omphacites. The high-*P* omphacites also show a higher K concentration and a lower Ca-Tschermaks component ($CaAlAlSiO_6$) than the low-*P* cpx. The Ca-Eskola component calculated from the proportion of vacancies (4.00 minus total cations) does not correlate with depth.

TEM foils were cut from optically clear volumes and from volumes with very fine optically visible inclusions. The secondary electron (SE) image in Figure 1a shows the surface of the (100) wafer of sample Ol-288/74. The wafer was mounted in crystal-bond, which allows cutting site specific TEM foils. Figure 1b shows an enlarged part of the crystal in Figure 1a with the now empty grooves where the TEM foils (1–3) were cut. The inclusions analyzed by AEM are of clinochlore composition (Table 3). However, lattice-fringe images and the diffraction patterns obtained from foils 1–3 indicate the presence of two phases: one with a *d*-spacing of about 14 Å, and the other with a *d*-spacing of about 7 Å. We identified the phases from the electron diffraction pattern as clinochlore (14 Å phase) and amesite (7 Å phase).

Amesite is chemically very similar to chlorite but belongs to the serpentine-group of minerals. It has a triclinic crystal structure with space group *C*1 (Hall and Bailey 1979). Because of its close relationship to chlorite, the name septechlorite has been proposed (Nelson and Roy 1958). The name septechlorite is synonymous with Al-rich serpentine and 7 Å chlorite (Bertoldi 2001). These serpentine-group minerals can occur at any composition that forms a chlorite (Deer et al. 1991). They can be differentiated by their strong basal reflection at about 7 Å and none at 14 Å. From clinochlore syntheses it is known that amesite is the primary phase, which then transforms to clinochlore at temperatures between 500 and 600 °C with time (months) (Bertoldi 2001). The close relationship between serpentine and chlorite minerals has also been observed in nature. It is well known that serpentine transforms to chlorite (and vice versa) and that random serpentine-chlorite intergrowth occur (Banfield and Bailey 1996).

The bright- and dark-field electron micrographs taken in the inclusion-rich part of the cpx (Figs. 1c and 1d) indicate that the sheet silicates show lattice-preferred orientation relationships. We also detected nanometer-sized inclusions in foil 3 taken from the optically clear part of sample Ol-288. However, due to the small size of the inclusions (interference with matrix) we were

TABLE 3. Composition of inclusions in Cpx obtained by AEM*

	Ol-288/74	O-175/87	TW-297/77	U-74
		wt% oxide		
MgO	35.65(362)	32.51(211)	34.36(181)	19.43(31)
Al_2O_3	26.55(311)	28.41(322)	27.44(196)	14.54(51)
SiO_2	35.26(125)	36.00(110)	36.22(86)	38.92(132)
K_2O	–	–	–	11.03(56)
TiO_2	–	–	–	0.47(15)
FeO†	2.54(52)	3.08(23)	1.99(47)	15.60(108)
Σ	100.00	100.00	100.00	100.00
		No. of oxygen		
atoms	14	22		
Mg	4.31(46)	3.92(35)	4.12(22)	4.16(7)
^{VI}Al	1.40(29)	1.62(29)	1.53(19)	0.04(9)
$^{IV}Al^{IV}$	1.14(9)	1.09(9)	1.08(7)	2.42(14)
Si	2.86(9)	2.91(9)	2.92(7)	5.58(14)
K	–	–	–	2.02(11)
Ti	–	–	–	0.05(2)
Fe*	0.17(4)	0.21(4)	0.13(3)	1.87(15)
Σ	9.87	9.74	9.78	16.14

* The analyses are normalized to 100%.
† Total Fe calculated as FeO.

TABLE 2. Electron microprobe analyses and structural formulae of Cpx

	U-935	U-74	Ol-288/74	0-175/87	Tw-140/79	Tw-297/77	Zg-25/78	A-45/2	2290	TM-8
					Wt% oxides					
Na_2O	1.59(7)	1.59(4)	3.39(7)	4.01(8)	4.42(5)	5.43(6)	5.20(4)	6.66(7)	8.28(7)	9.15(4)
Al_2O_3	12.68(46)	8.94(34)	17.67(10)	16.75(33)	8.50(12)	8.62(15)	3.55(10)	9.87(8)	16.20(11)	13.94(8)
MgO	10.75(17)	13.01(15)	9.04(7)	9.28(12)	10.29(7)	10.69(8)	8.62(5)	8.12(12)	5.92(5)	6.86(3)
SiO_2	48.77(23)	51.32(25)	49.16(14)	50.50(35)	54.99(27)	5.55(13)	5.22(15)	54.97(10)	57.28(19)	57.34(13)
CaO	22.09(16)	22.15(22)	20.16(13)	18.71(15)	17.06(13)	5.53(12)	14.88(7)	12.11(8)	10.20(9)	9.04(7)
K_2O	0.01(1)	0.01(1)	0.01(1)	0.02(1)	0.04(1)	0.06(1)	0.02(1)	0.08(1)	0.02(1)	0.04(1)
TiO_2	0.19(1)	0.21(2)	0.04(2)	0.06(2)	0.18(1)	0.33(2)	0.14(1)	0.43(1)	0.23(2)	0.40(2)
MnO	0.04(2)	0.02(1)	0.01(2)	0.01(1)	0.05(2)	0.04(2)	0.02(2)	0.01(2)	0.02(2)	0.05(3)
FeO*	4.09(6)	2.58(13)	1.34(8)	1.10(4)	5.00(8)	4.37(9)	2.44(9)	6.78(6)	2.68(5)	4.14(11)
Cr_2O_3	0.09(2)	0.10(2)	0.07(1)	0.10(2)	0.07(1)	0.07(2)	0.05(2)	0.10(2)	0.03(2)	0.03(1)
Σ	100.32	99.93	100.89	100.52	100.62	100.69	100.14	99.13	100.86	100.98
					Cations per 6 oxygen atoms					
Mg	0.583(9)	0.702(8)	0.478(4)	0.490(6)	0.549(2)	0.568(4)	0.452(3)	0.439(5)	0.305(3)	0.356(1)
Na	0.112(5)	0.112(3)	0.233(3)	0.275(4)	0.307(3)	0.375(4)	0.351(3)	0.468(3)	0.555(4)	0.618(2)
Al	0.543(20)	0.382(14)	0.739(3)	0.699(14)	0.359(6)	0.362(6)	0.562(4)	0.422(4)	0.660(4)	0.572(2)
Si	1.773(9)	1.858(7)	1.743(4)	1.787(9)	1.970(5)	1.978(2)	1.944(4)	1.994(2)	1.979(3)	1.997(3)
Ca	0.860(6)	0.859(8)	0.766(5)	0.710(5)	0.655(5)	0.593(5)	0.559(2)	0.471(2)	0.378(4)	0.337(2)
K	0.000(0)	0.000(0)	0.001(1)	0.001(1)	0.002(1)	0.003(1)	0.001(1)	0.004(1)	0.001(1)	0.002(1)
Ti	0.005(1)	0.006(1)	0.001(1)	0.002(1)	0.005(1)	0.009(1)	0.008(1)	0.012(1)	0.006(1)	0.010(1)
Mn	0.001(1)	0.001(1)	0.001(1)	0.000(0)	0.001(1)	0.001(1)	0.000(0)	0.000(0)	0.000(0)	0.001(1)
Fe*	0.124(2)	0.078(4)	0.040(2)	0.033(1)	0.150(3)	0.130(3)	0.072(3)	0.206(1)	0.077(1)	0.121(3)
Cr	0.003(1)	0.003(1)	0.002(1)	0.003(1)	0.002(1)	0.002(1)	0.002(1)	0.003(1)	0.001(1)	0.001(1)
Σ	4.005	4.000	4.002	3.999	3.999	4.020	3.949	4.019	3.962	4.017
□	–0.005	0.000	–0.002	0.001	0.001	–0.020	0.051	–0.019	0.038	–0.017
^{IV}Al	0.227	0.142	0.257	0.213	0.030	0.022	0.056	0.001	0.021	0.003
^{VI}Al	0.316	0.239	0.482	0.486	0.329	0.340	0.506	0.386	0.639	0.570
X_{Jd}	0.11	0.11	0.23	0.27	0.30	0.35	0.36	0.42	0.56	0.57
$X_{Ca\text{-}Tsch}$	0.22	0.14	0.26	0.21	0.03	0.02	0.06	0.06	0.02	0.00
P (GPa)	1.3–2.0	1.3–2.0	3.0	3.0	3.9–4.3	3.9–4.3	< 3.0	5.5	3.0	4.4

* Total Fe calculated as FeO.

not able to determine their composition. Fourier filtered lattice fringe images of such small inclusions indicate a fringe spacing of 14 Å or 7 Å. Because the inclusions show the same *d*-values of either 14 Å or 7 Å, we conclude that nanometer-sized chlorite and amesite inclusions also exist in the optically clear parts (Fig. 1e). TEM foils of samples Tw-297 and O-175 taken in inclusion-rich as well as optically clear parts also show the presence of chlorite and amesite similar in composition to sample Ol-288 (Table 3). The inclusions commonly appear as nanometer-sized nests or veins within the cpx (Figs. 1f and 1g). The chemical composition of inclusions in sample U-74 (Figs. 1h and 1i) and a lattice fringe spacing of 10.3 Å suggests that these inclusions are biotite. As for the mantle-derived omphacites described in the present study, such an alteration is very unusual. However, during uplift, the samples must have interacted with fluids. Due to its perfect cleavage, cpx behaves like a sponge soaking up fluids that produce alterations. In the inclusion-rich parts, we found not only enrichment in sheet silicates but also a relatively high concentration of fluid inclusions and, in some cases, a Cl-rich matrix between the sheet silicates. Because the grain size of the sheet silicates in the omphacites is very small, the analyses given in Table 3 certainly represent mixed compositions, which might explain the relatively large variability in composition.

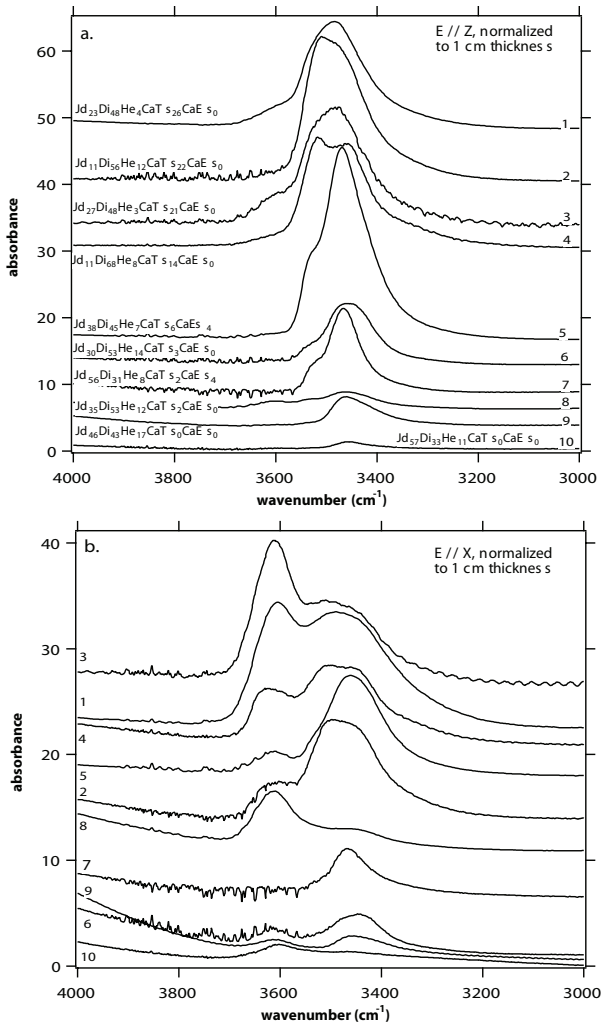

FIGURE 2. Polarized infrared spectra of cpx with **(a)** E // Z (n_γ) and **(b)** E // X (n_α). The labels correspond to the following samples 1 = Ol-288/74, 2 = U-935, 3 = O-175/87, 4 = U-74, 5 = Zg-25-78, 6 = Tw -140/79, 7 = 2290, 8 = Tw- 297/77, 9 = A-45/2, 10 = TM-8. The spectra are normalized to centimeter thickness and are offset for clarity.

OH incorporation

Polarized infrared spectra of the samples with E // Z (n_γ) and E // X (n_α) are shown in Figures 2a and 2b. The spectra with E // Y (n_β) are similar to those with E // X and are not presented here. All three groups of absorption bands described above can be distinguished in our spectra. The bands of groups 1 and 2 have their highest intensity with E // Z and those of group 3 with E // X. To check the homogeneity of the samples, we used synchrotron IR radiation and acquired unpolarized as well as polarized IR spectra with a spot size of 5 × 5 µm. We observed that the intensities of the absorption bands, mainly that of group 3, show extreme variation within one crystal (Figs. 3a, 3b, and 3c). In all cases, the strongest intensities were obtained in spots where we observed micrometer- to nanometer-sized crystalline inclusions in the cpx. Thus, it is questionable whether the bands of group 3 are related to intrinsic OH groups in omphacite.

There are several indications that the OH groups that are responsible for group 3 bands are not intrinsic: (1) There is no correlation between the intensity of the OH bands of band group 3 and the chemical composition of the cpx. Intense OH-stretching bands at 3610 cm^{-1} have been observed in augitic and diopsidic compositions but not in omphacite (Skogby et al. 1990). (2) The peak positions of group 3 bands are always the same as those of the inclusions (Fig. 3). Clinochlore, amesite, and biotite, which were found by TEM as inclusions in the cpx samples, do have prominent OH bands in this region (Vedder 1964; Welch et al. 1995; Velde 1980 and Fig. 4). The high-energy band in the clinochlore spectrum at 3610 cm^{-1} is due to a stretching vibration of OH groups within the octahedral sheet of the 2:1 layer (Ferrage et al. 2003). Those authors assign the much weaker OH-stretching band at 3475 cm^{-1} to interlayer hydroxyl. (3) The in-situ high-pressure IR measurements on omphacite and on synthetic clinochlore indicate that the shift of the bands of group 3 in omphacite with pressure is the same like that observed for clinochlore (Fig. 4). Fig. 4d even shows that the fine structure of the prominent OH band at 3610 cm^{-1} in the high-pressure spectrum of clinochlore (8 GPa) is identical to the fine structure of the OH band at the same position in the high-pressure spectrum of omphacite (9 GPa). (4) Spectra taken in inclusion-rich parts of the crystals show the same polarization dependence as spectra from optically clear parts (Figs. 5 and 6a). (5) It is known that pyroxene can be replaced by sheet silicates, and that the replacement can be topotactic with the sheets parallel to (100) planes of pyroxene and the **b** axes of both parallel to each other (Buseck et al. 1980). Such an orientation relationship between cpx and clinochlore would give an absorption maximum for the 3610 cm^{-1} band of clinochlore if the angle between the E vector of the polarized radiation and the **c**-axis of omphacite amounts to 60° in the (010) plates. This direction coincides with the X (n_α) direction in omphacite (see inlet below) and explains

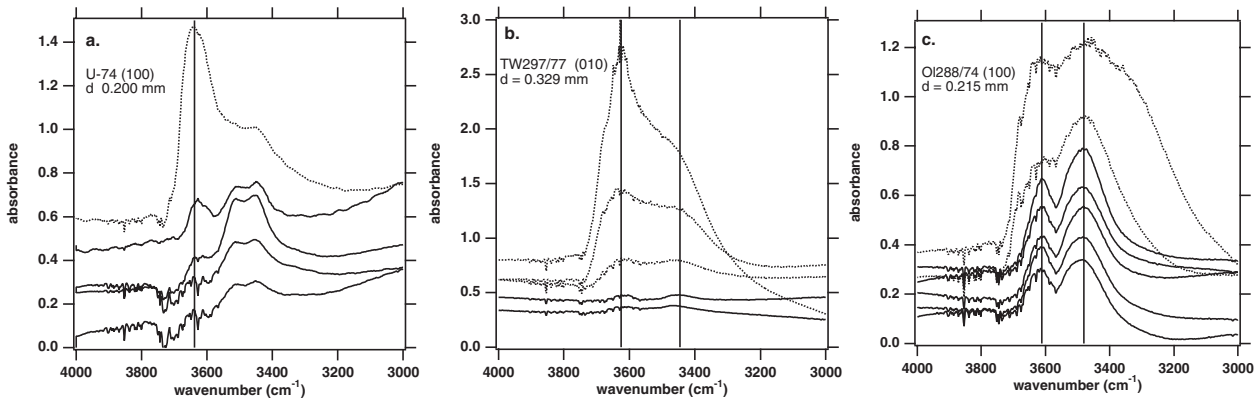

FIGURE 3. Unpolarized infrared spectra from different parts of one sample taken on optically clear (solid line) and on inclusion-rich (dotted line) parts with an aperture of 5 by 5 μm using synchrotron IR radiation.

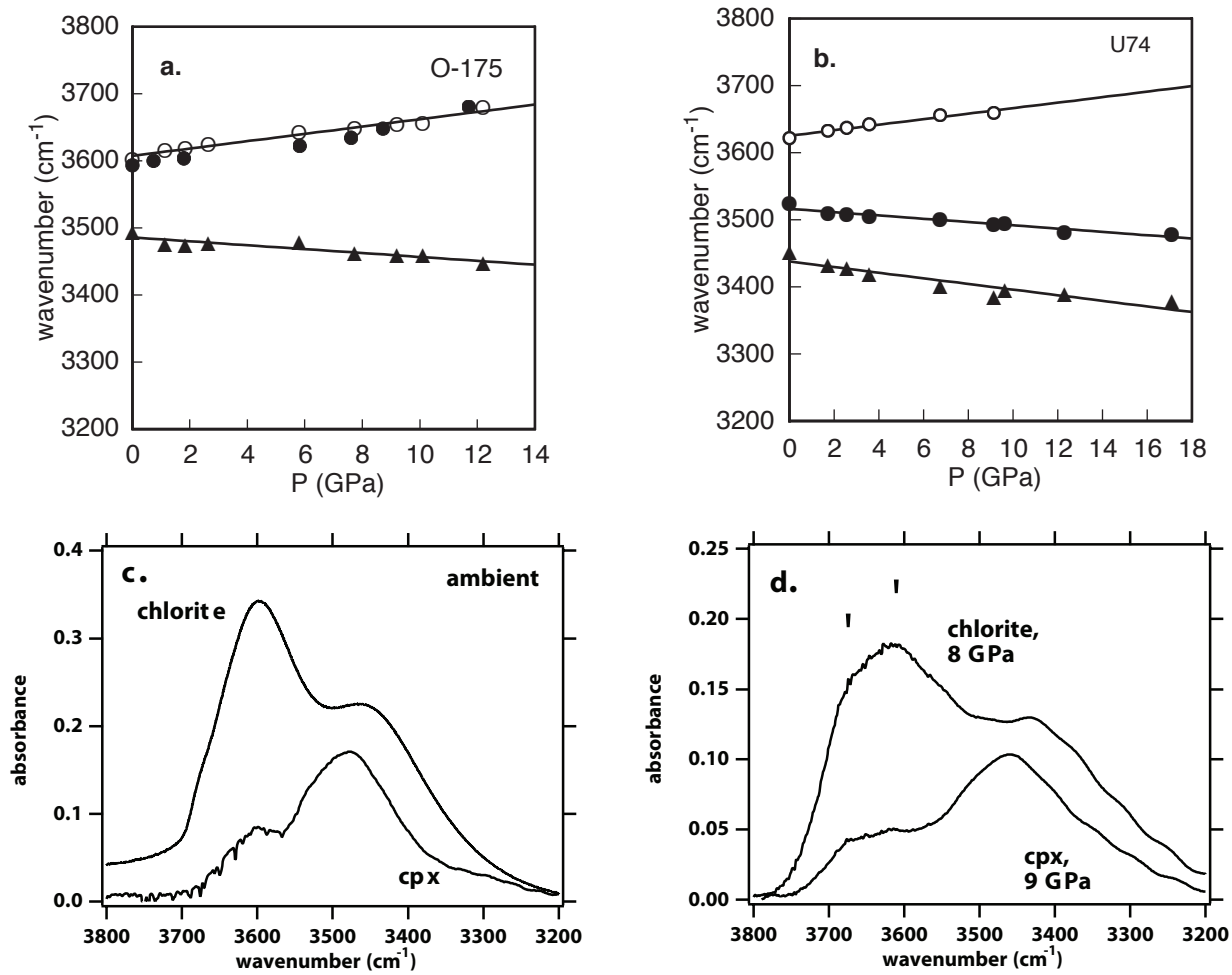

FIGURE 4. (a) Pressure shift of the OH bands of groups 1 and 2 (triangles) and group 3 (solid circles) of cpx samples O-175 in comparison to the pressure shift of the OH band of synthetic chlorite, 99-1 (open circles). **(b)** Pressure shift of the OH bands of groups 1 and 2 (triangles and solid circles, respectively) and of group 3 open circles of cpx sample U-74. **(c)** Unpolarized infrared spectra of cpx sample O-175 and chlorite sample 99-1 taken at ambient conditions. **(d)** Unpolarized infrared spectra of cpx sample O-175 and chlorite sample 99-1 taken in-situ at 9 and 8 GPa, respectively. The arrows indicate the fine structure of the intense chlorite OH band, which is also visible in the cpx spectrum.

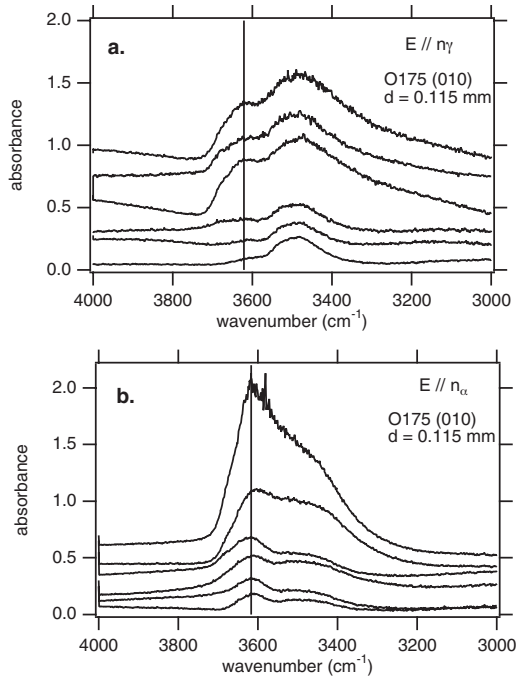

FIGURE 5. Polarized infrared spectra with **(a)** E // Z (n_γ) and **(b)** E // X (n_α) taken on different parts on the (010) wafer of cpx sample O-175 with a 5 × 5 µm aperture using synchrotron IR radiation.

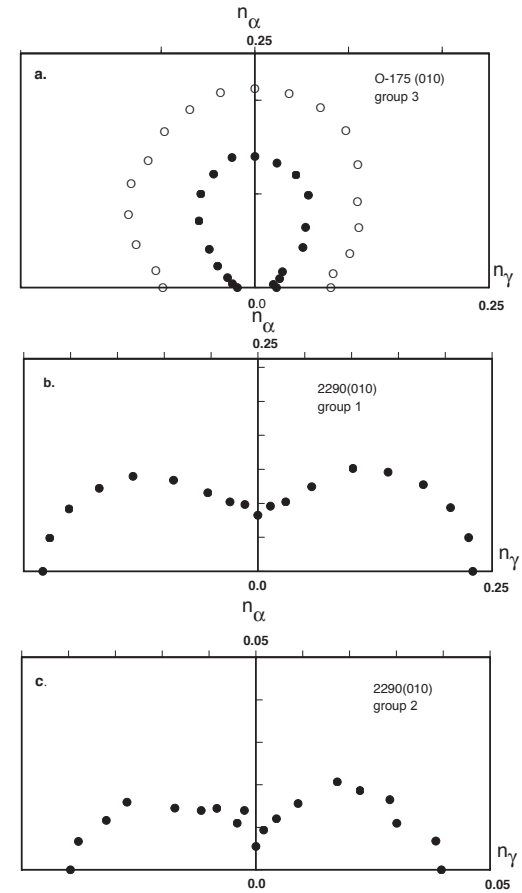

FIGURE 6. Linear absorbance of the OH-stretching bands in cpx taken on (010) wafers as a function of the orientation of the E vector of the incident radiation. **(a)** for group 3 bands taken on optically clear parts (solid circles) and inclusion-rich parts (open circles) of sample O-175. **(b, c)** for groups 1 and 2 bands taken on optically clear parts of sample 2990. The intensity of the OH-stretching band of group 3 is zero in the spectra of sample 2290.

the observed pleochroic behavior of the groups 3 bands.

Thus, we believe that the OH groups that cause the absorption bands of group 3 in omphacite and omphacitic cpx are not intrinsic but are related to nanometer-sized inclusions of sheet silicates within the crystals. The inclusions are due to alteration processes. We made the same observations on omphacites from the Roberts Victor kimberlite pipe, South Africa. As the omphacite IR-spectra published by Katayama and Nakashima (2003) also show strong absorption of group 3 bands, we strongly recommend that those samples be checked for the presence of nanometer-sized alteration products. According to our results, the proposed water content of 3000 ppm H_2O for the diamond-grade omphacite by Katayama and Nakashima (2003) could be overestimated by at least 30%.

It is known from TEM analyses that pyroxenes frequently alter to amphibole (see overview in Buseck et al. 1980). The presence of such intergrowths can easily be detected by IR spectroscopy through the presence of sharp "amphibole" bands around 3670 cm^{-1}. We found no indications of such alterations in any of our cpx samples either by TEM or by IR spectroscopy.

Incorporation of hydrogen into omphacite is suggested to occur through replacement of O^{2-} by OH^-, charge balanced by cation vacancies at M2 (e.g., Beran 1976; Cameron and Papike 1980; Smyth et al. 1991), and charge balanced by a charge-deficient substitutions such as incorporation of Al for Si (e.g., Skogby et al. 1990, Skogby 1994). The latter substitution amplifies the underbonded character of the O2 site and may be essential for OH incorporation in cpx (Skogby et al. 1990). As for our samples, the intensities and peak positions of the bands of group 2 correlate with the amount of tetrahedrally coordinated Al^{3+} (Figs. 7a and 7b). This result indicates that the OH groups, which are responsible for group 2 bands, must be related to tetrahedral Al. The vacancy concentration of the cpx of this study correlates fairly well with the intensities and peak positions of the bands of group 1 (Figs. 7c and 7d, Table 2). The negative values for the vacancy concentrations may be due to the presence of Fe^{3+}, which we neglected in the calculations. ^{57}Fe Mössbauer spectroscopy on mantle-derived cpx from other mantle xenoliths contained 18–22% of the total Fe as Fe^{3+}(e.g., Dyar et al. 1989). If we apply this value to the cpx samples of our study, the total amount of Fe^{3+} cations would range from 0.006 to 0.041 per formula unit (pfu). This relatively low amount would not affect the cations pfu given in Table 1 in a serious way, but it would affect the calculated vacancy concentration. If Fe^{3+} were present in an equal amount in all samples of this study, the slopes of the correlation shown in Figures 7c and 7d would be the same as

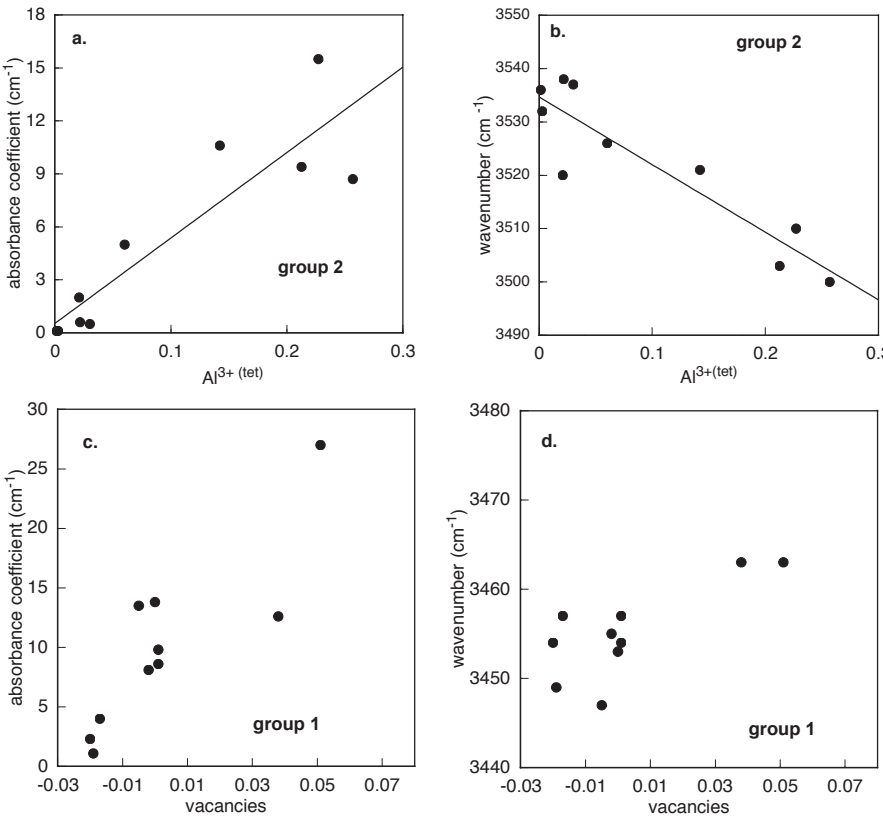

FIGURE 7. (a, b) Plots of linear absorbance normalized to 1 cm of the n_γ-polarized absorption peaks of the bands of group 2 of cpx and plot of the wavenumber of the bands of group 2 of cpx as a function of tetrahedrally coordinated Al^{3+}. **(c, d)** Plots of linear absorbance normalized to 1 cm of the n_γ-polarized absorption peaks of the bands of group 1 of cpx and of the wavenumber of the bands of group 1 of cpx as a function of the vacancy concentration, calculated as 4 minus total cations per 6 oxygen atoms.

shown but the vacancy concentration would be shifted to higher values. According to McCormick (1986), vacancies in cpx occur at the M2 site. Thus, the correlations in Figures 7c and 7d indicate that cation vacancies at M2 control the incorporation of the OH groups responsible for the bands of group 1.

The exact locations of the OH ions in the pyroxene structure are not known precisely (Skogby 1994). From polarized IR spectra, Beran (1976) and Skogby et al. (1990) concluded that the OH groups that cause the OH-stretching bands of groups 3 in diopside substitute for the O2 oxygen and point directly toward an O3 oxygen. According to Skogby et al. (1990), the OH groups that cause the OH-stretching bands of groups 1 and 2 are also caused by substitution for O2 but point in another (not specified) direction. This conclusion is in contrast to the findings of Smyth et al. (1991) who suggested that the OH groups that cause groups 1 and 3 absorption bands point in the same direction. Analyses of our polarized and high-pressure IR spectra may help to locate the H atoms. The bands of groups 1 and 2 exhibit the same polarization dependence (Figs. 2, 6b, and 6c) and the same pressure dependence (Fig. 4b) but occur at different wavenumbers. Thus, they must be caused by the same types of OH dipoles occurring in different structural environments. The absorbance figures for the group 1 and group 2 bands of our samples all show the same shape with maximum and minimum absorbances parallel to the indicatrix axes (Figs. 6b and 6c). In the case of cpx, which crystallizes in monoclinic symmetry, however, one type of OH dipole alone cannot explain the observed polarization behavior. If there were just one OH dipole, e.g., parallel to n_γ, the absorbance figure of an (010) plate would be similar to that shown by Beran (1976) for diopside with maximum absorbance with E // n_γ and zero absorbance with E // n_α. The absorbance figures shown in Figures 6b and 6c resemble those of higher symmetry crystals, where symmetry related absorbers summing up their single absorbances to minimum and maximum values along the three indicatrix axes (Libowitzky and Rossman, 1996). However, from single crystal X-ray diffraction (V. Kahlenberg, pers. comm.) there is no doubt about the monoclinic symmetry of these crystals (space group *C*2/*c*). The only explanation for our observation is that there must be two different hydrogen positions but with identical O-H···O distances and environments. To explain the polarization behavior, we propose two hydrogen atoms, H1 and H2, bonded to O2 and pointing not directly to the acceptor oxygen O2 but with a O-H···O angle of about 160–170° (Fig. 8). Such an orientation of the OH dipoles is consistent with the observed polarization dependence of the bands in the spectra with E // n_α, n_β, and n_γ. The two H positions around one O2 are not simultaneously occupied but their site-occupancy factor should be similar. The O2···O2 distance is 3.14 Å, an acceptable value for the observed wavenumbers of the bands. The OH bands of group 2 are now explained by vibrations of both dipoles O2-H1···O2 and O2-H2···O2 when the neighboring Si is substituted by Al. The distances of Si-H1 and Si-H2 are identical in our model and have an acceptable value of 1.65 Å. The OH bands of group 1 are assigned to vibrations of the same dipoles when the neighboring M2 site is vacant. A vacant M2 site is larger than a filled one and thus would decrease the O2···O2 distances, which would lower the corresponding vibrational energy and result in a decrease of the corresponding wavenumber.

Quantification of the structural bonded OH

The content of structurally bound water in the omphacites and omphacitic cpx ranges from 31–514 ppm H_2O (Table 1). The lowest contents were found in the region that experienced the highest pressure, i.e., for the diamond-bearing eclogite xenoliths of the Mir kimberlite pipe. The largest values were obtained for omphacites of the lower pressure grospydites of the Zagadochnaya kimberlite pipe and for the omphacitic cpx of the granulites of the Udachnaya kimberlite pipe. This observation is somehow surprising as it is at variance with the findings worldwide, i.e., that the upper-mantle cpx carry the highest concentrations of H. The controlling factors for H incorporation or H loss in mantle-derived nominally anhydrous minerals (NAMs) has been worked out in detail by e.g., Skogby et al. (1990), Rossman (1996), Matsyuk et al. (1998), Ingrin and Skogby (2000). Matsyuk et al. (1998) summarized the most prominent factors that may control the total amount of $(OH)^-$ defects found in garnet from mantle xenoliths as: (1) internal factors, such as solubility and diffusivity of H constrained by crystal chemistry and structure; (2) factors related to the intercrystalline distribution of H; and (3) external factors such as H_2O-, H_2 and/or O_2 fugacity, *P*, *T*, and rate of uplift. They found that the OH contents of garnets from kimberlites of the Siberian platform vary widely, being significantly lower in garnet formed in high-pressure/high-temperature diamond-pyrope facies compared to garnets formed under the conditions of the graphite-pyrope facies. Considering the above-mentioned constrains, Matsyuk et al. (1998) concluded that the low water contents in garnets are related to significantly lower water activity in the higher-pressure rocks as compared with the lower-pressure rocks under the Siberian platform. This conclusion is consistent with fluid inclusion data (e.g., Tomilenko et al. 1997). Our results on omphacite seem to be consistent with this conclusion. On the other side, how do we know that all H in omphacite did survive the transport to the surface during the uplift (Rossman 1996)?

Experimental data show that diffusion of H in NAMs is so fast that H loss can occur in a matter of hours (e.g., Skogby and Rossman 1989; Mackwell and Kohlstedt 1990; Ingrin et al. 1995). The mechanism that is generally assumed to control H loss in Fe-bearing systems involves oxidation of the Fe^{2+} according to $Fe^{3+} + O^{2-} + 1/2\ H_2 = Fe^{2+} + OH^-$. Ingrin and Skogby (2000) proposed on the basis of published Fe^{3+} contents of cpx that the initial H concentration in upper-mantle clinopyroxenes may be about two times higher than the actually observed upper values. Actually, the cpx of our study with the lowest water content and the highest crystallization pressure shows the highest "negative" cation vacancy values, which could indicate significant Fe^{3+} incorporation. Further systematic studies of the relation between H and Fe^{3+} contents in mantle-derived omphacite are needed.

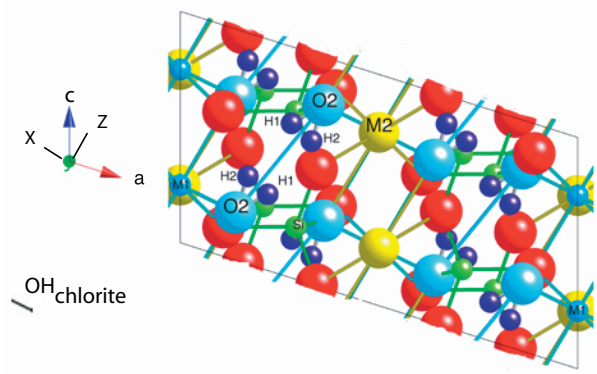

FIGURE 8. Part of the clinopyroxene structure in space groups *C*2/*c* showing the proposed H1 and H2 hydrogen atoms. The Z (n_γ) direction is parallel to the O2···O2 bond. Also shown is the orientation of the intralayer OH-dipole of the clinochlore inclusions causing the high energy band at 3610 cm^{-1}. We used the structural data of Zheng and Bailey (1989) and the orientation relationship for clinochlore and omphacite as proposed by Buseck et al. (1980).

ACKNOWLEDGMENTS

We thank U. Schade who helped with the synchrotron measurements at Bessy II, Berlin, Germany, Z. Spetsius who provided us with the samples U-935, U-74, and 2290, and D. Radny, GFZ Potsdam, who helped in the preparation and infrared measurements of the samples. We thank N.V. Sobolev for helpful suggestions and discussions and I. Katayama for providing a preprint of his paper on omphacites. The comments of the reviewers G. Rossman and R. Stalder helped to improve the manuscript.

REFERENCES CITED

Banfield, J.F. and Bailey, S.W. (1996) Formation of regularly interstratified serpentine-chlorite minerals by tetrahedral inversion in long-period serpentine polytypes. American Mineralogist, 81, 79–91.

Bell, D.R., Ihinger, P.H. and Rossman, G.R. (1995) Quantitative analysis of trace OH in garnet and pyroxenes. American Mineralogist, 80, 465–474.

Beran, A. (1976) Messung des Ultrarot-Pleochroismus von Mineralen. XIV. Der Pleochroismus der OH-Streckfrequenz in Diopsid. Tschermaks Mineralogische-Petrographische Mitteilungen, 23, 79–85.

Beran, A., Langer, K. and Andrut, M. (1993) Single crystal infrared spectra in the range of OH fundamentals of paragenetic garnet, omphacite and kyanite in an eclogitic Mantle Xenolith. Mineralogy and Petrology, 48, 257–268.

Bertoldi, C. (2001) Thermochemische Eigenschaften von Chloritgruppenmineralen $(Mg, Fe, Al)_{12}[(Si, Al)_8O_{20}](OH)_{16}$. Dissertation, Naturwissenschaften, Paris Lodron Universität Salzburg, Austria.

Bromiley, G.D. and Keppler, H. (2003) Solubility and speciation of hydrogen in jadeite and Na-rich pyroxenes under upper-mantle conditions. Geophysical Research Abstracts, 5, 03211, 2003.

Buseck, P.R., Nord, G.L., Jr., and Veblen, D.R. (1980). Subsolidus phenomena in pyroxenes. In C.T. Prewitt , Ed, Pyroxenes. Reviews in Mineralogy, 7, 117–211.

Cameron, M. and Papike, J.J. (1980) Crystal chemistry of silicate pyroxenes. In C.T. Prewitt, Ed., Pyroxenes. Reviews in Mineralogy, 7, 1–93.

Deer, W.A., Howie, R.A. and Zussman, J. (1991) An introduction to the rock-forming minerals. Longman Scientific & Technical, Essex, UK.

Dyar, M.D., McGuire, A.V., and Ziegler, R.D. (1989) Redox equilibria and crystal chemistry of coexisting minerals from spinel lherzolite mantle xenoliths. American Mineralogist, 74, 969–980.

Ferrange, E., Martin, F., Micoud, P., Petit, S., de Parseval, P., Beziat, D., and Ferret, J. (2003) Cation site distribution in clinochlores: a NIR approach. Clay Minerals, 38, 329–338.

Hall, S.H. and Bailey, S.M. (1979) Cation ordering pattern in amesite. Clays and Clay Minerals, 27, 241–247.

Heaney, E.P., Vicenzi, E.A., Giannuzzi, L.A., and Livi, K.J.T. (2001) Focused ion beam milling: a method of site-specific sample extraction for microanalysis of Earth and planetary materials. American Mineralogist, 86, 1094–1099.

Ingrin, J. and Skogby, H. (2000) Hydrogen in nominally anhydrous upper-mantle minerals: concentration levels and implications. European Journal of Mineralogy, 12, 543–570.

Ingrin, J., Hercule, S., and Charton, T. (1995) Diffusion of hydrogen in diopside: Results of dehydration experiments. Journal of Geophysical Research, 100, 15489–15499.

Katayama, I. and Nakashima, S. (2003) Hydroxyl in clinopyroxene from the deep subducted crust: evidence for H_2O transport into the mantle. American Mineralogist, 88, 229–234.

Koch-Müller, M. and Wirth, R. (2001) An experimental study of the effect of iron on magnesiochloritoid-talc-clinochlore-kyanite stability. Contributions to Mineralogy and Petrology, 141, 546–559.

Libowitzky, E. and Rossman, G.R. (1996) Principles of quantitative absorbance measurements in anisotropic crystals. Physics and Chemistry of Minerals,

23, 319–327.
——— (1997) An IR absorption calibration for water in minerals. American Mineralogist, 82, 1111–1115.
Mackwell, S.J. and Kohlstedt, D.L. (1990) Diffusion of Hydrogen in Olivine: Implications for water in the mantle. Journal of Geophysical Research, 95, 5079–5088.
Mao, H.K., Xu, J., and Bell, P.M. (1986) Calibration of the Ruby pressure gauge to 800 kbar under quasi-hydrostatic conditions. Journal of Geophysical Research, 91, 4673–4676.
Mao, H.-K. and Hemley, R.J. (1998) New windows on the earth's deep interior. In R.J. Hemley, Ed., Ultrahigh-Pressure Mineralogy. Review in Mineralogy, 37, 1–32.
Matsyuk, S.S., Langer, K., and Hösch, A. (1998) Hydroxyl defects in garnets from mantle xenoliths in kimberlites of the Siberian platform. Contribution to Mineralogy and Petrology, 132, 163–179.
McCormick, T.C. (1986) Crystal-chemical aspects of nonstoichiometric pyroxenes. American Mineralogist, 71, 1434–1440.
Nelson, B.W. and Roy, R. (1958) Synthesis and stability of minerals in the system MgO-Al_2O_3-SiO_2-H_2O. American Mineralogist, 40, 147–178.
Overwijk, M.H.F. and van den Heuvel, F.C. (1993) Novel scheme for the preparation of transmission electron microscopy specimens with a focused ion beam. Journal of Vacuum Science and Technology, B 11, 2021–2024.
Peslier, A.H., Luhr, J.F., and Post, J. (2002) Low water contents in pyroxenes from spinel-peridotites of the oxidized, sub-arc mantle wedge. Earth and Planetary Science Letters, 201, 69–86.
Pouchou, J.L. and Pichoir, F. (1985) "PAP" φ (ρZ) procedure for improved quantitative microanalysis. Microbeam Analyses, 1985, 104–106.
Qu, Q., Taylor, L.A., Snyder, G.A., Clayton, R.N., Mayeda, T.K., and Sobolev, N.V. (1997) Detailed petrology and geochemistry of a rare corundum eclogite xenolith from Obnazhennaya pipe. Geologiya i Geofizika, 38, 233–244. (in Russian)
Raheim, A. and Green, D.H. (1974) Experimental determination of the temperature and pressure dependence of the Fe-Mg partition coefficient for coexisting garnet and clinopyroxene. Contribution to Mineralogy and Petrology, 48, 179–203.
Rossman, G.R. (1996). Studies of OH in nominally anhydrous minerals. Physics and Chemistry of Minerals, 23, 299–304.
Skogby, H. (1994) OH incorporation in synthetic clinopyroxene. American Mineralogist, 79, 240–249.
Skogby, H. and Rossman, G.R. (1989) OH^- in pyroxene: An experimental study of incorporation mechanisms and stability. American Mineralogist, 74, 1059–1069.
Skogby, H., Bell, D.R., and Rossman, G.R. (1990) Hydroxide in pyroxene: Variations in the natural environment. American Mineralogist, 75, 764–774.
Smyth, J.R. (1989) Electrostatic characterization of oxygen sites in minerals. Geochimica and Cosmochimica Acta, 53, 1101–1110.
Smyth, J.R., Bell, D.R., and Rossman, G.R. (1991) Incorporation of hydroxyl in upper-mantle clinopyroxenes. Nature, 351, 732–735.
Sobolev, N.V. (1974) Deep-seated inclusions in kimberlites and the problem of the composition of the upper mantle. Nauka, Novosibirsk (p. 264) (in Russian)
Spetsius, Z.V. (1990) Megaxenolith of coesite Eclogite from the Udachnaya kimberlite pipe. Doklady Akademii Nauk SSSR vol. 313, N1, p. 153–157 (in Russian)
Spetsius, Z.V. and Serenko, V.P. (1990) Composition of continental upper mantle and lower crust beneath the Siberian platform, 272 p. Nauka, Moscow, (in Russian).
Tomilenko, A.A., Chepurov A.L., Pal'yanov Y.N., Pokhilenko, L.N., and Shebanin, A.P. (1997) Volatile components in the upper mantle (from data on fluid inclusions). Geologiya i Geofizika, 38, 276–285 (in Russian).
Ukhanov, A.V., Ryabchikov, I.D., and Kharkiv, A.D. (1988) Lithospheric mantle of the Yakutian kimberlite province, 286 p. Nauka, Moscow, (in Russian).
Vedder, W. (1964) Correlations between infrared spectrum and chemical composition of mica. American Mineralogist, 49, 736–768.
Velde, B. (1980) Ordering in synthetic aluminous serpentines; infrared spectra and cell dimensions. Physics and Chemistry of Minerals, 6, 209–220.
Welch, M.D., Barras, J., and Klinowski, J. (1995) A multinuclear NMR study of clinochlore. American Mineralogist, 80, 441–447.
Zheng, H. and Bailey, S.W. (1989) Structures of intergrowth triclinic and monoclinic II b chlorites from Kenya. Clays and Clays Minerals, 37, 308–316.

MANUSCRIPT RECEIVED OCTOBER 6, 2003
MANUSCRIPT ACCEPTED FEBRUARY 8, 2004
MANUSCRIPT HANDLED BY SIMON KOHN